



## Experimental Investigations to Detection of Liver Cancer Using ResUNet

Koteswara Rao Kodepogu<sup>\*</sup>, Sandhya Rani Muthineni, Charisma Kethineedi, Jasthi Tejesh, Joshitha Sai Uppalapati

Department of CSE, PVP Siddhartha Institute of Technology, Vijayawada, Andhra Pradesh 520007, India

Corresponding Author Email: [kkrao@pvpsiddhartha.ac.in](mailto:kkrao@pvpsiddhartha.ac.in)

<https://doi.org/10.18280/ts.400548>

### ABSTRACT

**Received:** 2 December 2022  
**Revised:** 25 August 2023  
**Accepted:** 13 October 2023  
**Available online:** 30 October 2023

#### Keywords:

*U-Net, CT images, ROI, ResUNet*

The detection and identification of cancerous tissue is currently a time-consuming and challenging process. The segmentation of liver lesions from cancer CT images can aid in treatment planning and clinical response monitoring. This study employs Residual U-Net, a powerful tool that has been adapted and applied for the segmentation of liver tumors, addressing the ongoing challenge in liver cancer diagnosis. Segmentation of liver lesions in CT images can be utilized to assess tumor burden, predict therapeutic outcomes, and monitor clinical response. In this research, the liver was extracted from the CT image using ResUNet, and the tumor was subsequently segmented using another ResUNet applied to the extracted Region of Interest (ROI). This approach effectively extracts features from Inception by combining residual and pre-trained weights. The deep learning system elucidates the underlying concept by highlighting the components contributing to the inner layer analysis and prediction, and by revealing a section of the decision-making process employed by pre-trained deep neural networks.

## 1. INTRODUCTION

### 1.1 Liver anatomy

The liver, a vital organ in the digestive system, comprises two lobes. Although it performs various functions, its primary role is to process the nutrients absorbed by the small intestine. Additionally, the liver produces bile juice, which it delivers to the small intestine, facilitating the breakdown of fats. The body leverages the raw materials ingested by the gut, enabling the liver to synthesize essential chemicals for its operation and to remove hazardous substances from the body [1]. Figure 1 shows the anatomy of the liver.

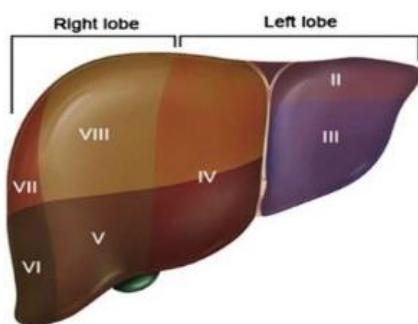


Figure 1. Anatomy of the liver

### 1.2 Liver tumors and stages

Statistics reveal that liver cancer ranks as the second most lethal disease in men and the sixth most prevalent cancer in women. Approximately 750,000 individuals were diagnosed with liver cancer in 2008, and of those, 696,000 succumbed to the disease. Globally, male infection rates are double those of

females. The highest incidence rates are observed in East and South-East Asia, and Middle and Western Africa. While the prevalence of this disease is widespread, there is a notable increase in the United States and Central Europe. This rise may be attributed to obesity, the spread of the Hepatitis C virus (HCV), and the increasing incidence of liver cancer [2]. Figures 2-5 illustrate the various stages of liver tumors, along with the corresponding diagnosis and treatment procedures required for each stage [3].

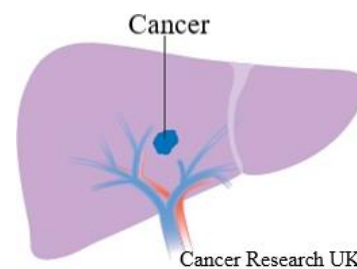


Figure 2. Stage 1A of liver tumors

### 1.3 Computed tomography CT

Diagnostic methodologies have significantly evolved since the introduction of computer tomography (CT) in the 1970s. CT scanning has improved the detection of cancer, facilitated surgical procedures, enhanced radiation therapy, and advanced the monitoring of cardiac conditions, thereby eliminating the need for exploratory surgeries [4].

Unlike traditional x-ray machines which utilize a fixed x-ray tube, CT scanners employ a motorized x-ray source encircled by a gantry. The x-ray tube rotates around the patient while they lay on a bed that moves through the gantry. With the transition from film-based to digital x-ray detectors, CT

scanners can process the data to create a 2D image slice of the patient using the information gathered from one rotation. Moreover, the computer can generate a 3D representation of the patient by rotating the model in space and examining the slices sequentially. This 3D image displays all the scanned organs, aiding medical professionals in pinpointing the exact location of the problem [5].

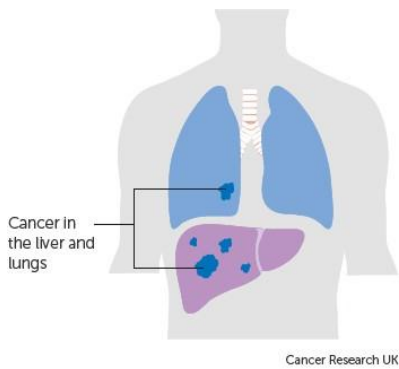


Figure 3. Stages 2A & 2B of liver tumors

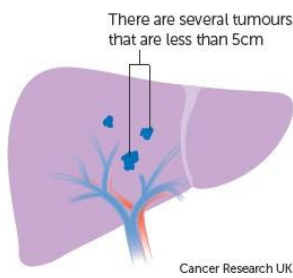


Figure 4. Stages 3A & 3B of liver tumors

### 1.4 Current state of liver tumor segmentation

Liver CT scans are commonly evaluated through manual or semi-manual methods. However, these approaches are often subjective, costly, time-consuming, and highly prone to errors. To address these challenges and enhance the accuracy of liver tumor diagnosis, several computer-aided methods have been developed. Yet, due to a range of issues such as minimal color contrast between the liver and lesions, proximity of other organs to the liver and tumors, varying contrast levels within tumors, variability in the number and size of tumors, tissue

abnormalities, and irregular tumor growth in response to drug treatments, these systems have not been highly effective at segmenting the liver and lesions. Consequently, a novel approach is required to surmount these obstacles.

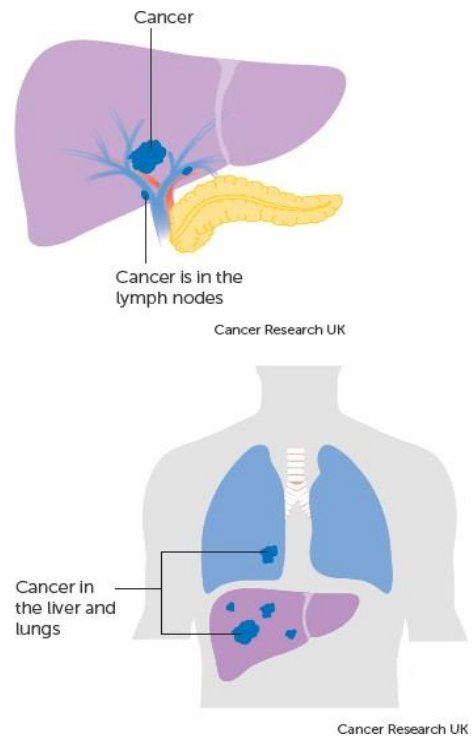


Figure 5. Stages 4A & 4B of liver tumors

### 1.5 Objective

The primary objective is to segment the liver and identify the lesion therein. This can be accomplished through three steps:

1. Augment the 3D-IRCADb01 Dataset.
2. Construct and train a ResUNet model to segment the liver.
3. Construct and train a ResUNet model to segment the tumors.

## 2. LITERATURE SURVEY

Bai et al. [6] proposed the Multi-scale Candidate Generation (MCG) for CT image-based liver tumor segmentation. To refine the detection of liver cancer cells, they employed a 3D fractal residual network and an active contour model. They performed segmentation tasks using the 3DIRCADb dataset, and the results, along with comparisons with related studies, demonstrate that their sophisticated system can achieve high segmentation efficiency.

Das et al. [7] suggested a deep learning-based Watershed Transform and Gaussian Mixture Model (WT-GMM) for liver cancer detection. This strategy relies on the marker-controlled alteration of the watershed and the Gaussian mixture model for accurate detection. The proposed method was tested in a real-time clinical setup using clinical data from a variety of patients. Their deep neural network classifier achieved an impressive accuracy of 99.38% with minimal validation loss, which is a significant advantage of this automated detection method.

Chlebus et al. [8] discussed liver lesion detection using 2D Convolutional Deep Neural Networks followed by shape-

based post-processing. They achieved an accuracy of 77% and state-of-the-art results on the LiTS challenge. A Random Forest classifier was trained on the features produced from the Convolutional Neural Network to filter False Positives, achieving an accuracy of 87%.

Li et al. [9] minimized the use of a Gaussian smoothing filter to reduce noise in CT scans. The resulting images were then normalized and down-sampled to expedite training time. The pre-processed images were then provided to the CNNs. They created 5 CNNs with different patch sizes:  $13 \times 13$ ,  $15 \times 15$ ,  $17 \times 17$ ,  $19 \times 19$ . However, the  $17 \times 17$  model outperformed all the other CNNs, thus proving to be the optimal choice.

Ben-Cohen et al. [10] utilized Fully Convolutional Networks (FCNs) in liver segmentation and detection of metastases from Computed Tomography (CT) scans. They tested their model on a small dataset composed of 20 patients with a total of 68 lesions and 43 livers in one slice, along with 20 different patients for 3D liver segmentation. After cross-validation, they achieved promising results with a true positive rate of 0.86 and 0.6 false positives per patient. Following data augmentation, they trained two networks: one for liver segmentation, which isolated the liver from neighboring organs, and another for tumor and lesion segmentation, which operated on the output of the first network.

Christ et al. [11] proposed a method to automatically segment the liver and lesions from both MRI and CT abdominal images using two cascaded Fully Convolutional neural Networks (CFCNs). One network was used for liver segmentation and the other for detecting lesions from the Region of Interest (ROI) resulting from the first CFCN. They used the models on a clinical dataset for DW-MRI, with clinical evaluation and MR imaging performed on 31 patients for the primary diagnosis of HCC. The cascaded U-Net achieved an 87% dice score for liver in MR-DWI and a mean dice score of 69.7% for lesions.

Goryawala et al. [12] proposed a novel 3D-segmentation method combining a modified k-means algorithm with a localized contouring algorithm. This method identified five distinct regions in the CT images during the segmentation step. Combined with 3D-rendering, the method proved to be fast and accurate, achieving a mean accuracy of 98.27%.

Milletari et al. [13] proposed a method for segmenting medical images that used Fully Convolutional Neural Networks (FCNNs). The FCN was trained end-to-end to process MRI volumes using volumetric convolutions instead of preprocessing the input volumes in a slice-wise manner. They proposed a novel objective function that maximizes the Dice coefficient, demonstrating accurate and fast results on prostate MRIs.

Yuan [14] worked on road extraction from aerial images, a fundamental but challenging task in remote sensing due to noise in aerial images. Road extraction has various applications, such as unmanned vehicle navigation, map plotting, and updating geographical data. They developed a new model, ResUNet, after failing to achieve optimal results with the U-Net model. ResUNet combines the benefits of both the ResNet and U-Net models. It employs residual blocks with skip-connections instead of the conventional convolutions used by the standard U-Net, enabling faster training with less data.

## 2.1 Research gaps

The computational complexity of the task is estimated using

the Gaussian Mixture Model, which requires less computation and fewer overall CT scans. The process could be further enhanced by incorporating 3D visualization of volumetric images in cancer detection. That is the main limitation of this type. Multi-scale Candidate Generation (MCG) cannot segment the cancer borders accurately because multiple adjacent tumors may merge into a single tumor region. These models primarily focused on cancer detection rather than accurately segmenting the tumor.

## 2.2 Problem statement

Generally, cancer detection involves the collection of organ tissue. However, the challenge is that when tissues are obtained through medical procedures, there's a risk of spreading cancer cells, which could worsen the condition. In this project, we aim to segment cancer cells based on CT scan images to minimize this risk.

CT scans are invaluable not only for designing treatment plans but also for monitoring clinical outcomes. The computational complexity of the task is estimated using the Gaussian mixture model, which requires less computation and fewer overall CT scans. To address these issues and enhance the accuracy of liver cancer diagnoses, we utilize Convolutional Neural Networks (CNNs). These networks have demonstrated effective results in image classification and face recognition tasks. Deep learning is often a rapid and straightforward method for aligning pixels in an image. The type of features returned for pre-processed images dictates the precision required for the task, and the extracted images can therefore reflect the features of the original images [15].

Our main goal is to develop a liver segmentation model. We will then use the Region of Interest (ROI) from this model to identify the liver tumor.

## 2.3 Deep learning models

Deep learning, a subset of machine learning, draws inspiration from the biological nervous system, particularly the sections responsible for data processing and communication. Among many learning architectures in deep learning, deep neural networks are a significant component.

These networks can be trained using various methods including supervised, semi-supervised, or unsupervised learning, depending on the task and available data.

Deep learning is versatile and has been successfully applied to a wide range of tasks, including speech recognition, computer vision, natural language processing, and medical image analysis. The network models are:

- Convolutional neural network
- U-Net
- ResNet

## 2.4 Convolutional neural network

Convolutional Neural Networks (CNNs) are structured similarly to traditional neural networks, as they are composed of neurons. Each neuron processes a weighted sum of multiple inputs it receives, and this result is then passed through an activation function to produce an output.

Like their counterparts, CNNs also utilize loss functions. However, unlike traditional neural networks that operate on vectors, CNNs operate on volumes. This is largely due to their unique architecture, which includes convolutional layers.

These convolutional layers comprise a collection of distinct filters that collectively process the input image. Each filter in the convolutional layer is responsible for extracting different features, making CNNs particularly effective for tasks involving image and pattern recognition.

### 2.5 U-Net architecture

The network architecture is shown in Figure 6. It consists of a contracting path and an expansive path and it consists of a total of 23 convolution layers [15, 16].

Every step in the Contracting Path shares a typical architecture of CNNs which consists of:

- Repeated two 3×3 convolutions;
- A Rectified Linear Unit (ReLU) refer to following every convolution. See figure for more details on ReLU;
- 2×2 max pooling operation with a stride of 2. See figure for more details on ReLU;

Down sampling where the number of feature channels is doubled Every Step in the Expansive Path consists of:

- Up sampling of the feature map;
- 2×2 convolution which decrease the size of feature maps by half;
- Concatenation with the cropped feature map;
- Two 3×3 convolutions;
- ReLU activation function [16].

### 2.6 U-Net limitations

While the U-Net model yielded impressive results on the liver segmentation images [17], it performed poorly on tumor segmentation, resulting in empty masks. After extensive research and testing, we discovered the Residual U-Net (ResUNet) model, which combines elements of both the U-Net and ResNet models [18, 19]. Figure 7 shows the segmentation result of the U-Net model.

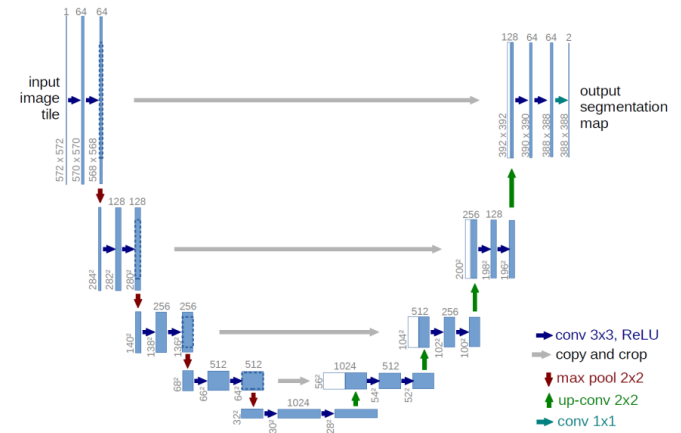


Figure 6. Architecture of the U-Net CNN

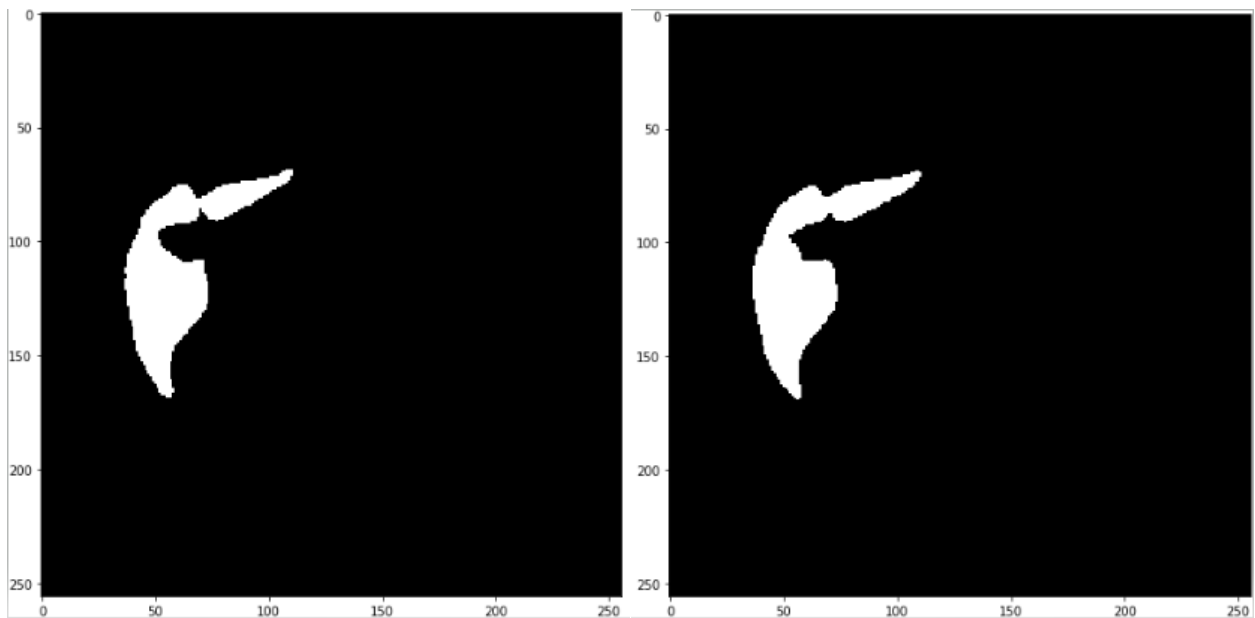


Figure 7. Random sample #1

### 2.7 ResNet

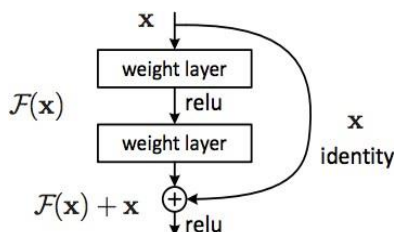


Figure 8. Residual block

ResNet, a variation of traditional Artificial Neural Networks, introduces a small but significant change called Residual

Blocks to the standard architecture. The core building blocks of ResNets, these Residual Blocks, leverage a crucial concept called Skip Connections. The main purpose of Skip Connections is to link a layer directly with a layer that is not its immediate successor [20, 21].

By bypassing a few layers during the initial stages of training, the network is simplified, which accelerates learning. This approach also mitigates the impact of the Vanishing Gradient problem, as there are fewer layers for the information to traverse. Residual blocks reuse the activation function from earlier layers to learn weights, and then adjust to amplify the skipped layer and dampen the upstream layer [22, 23]. While ResNets typically skip only one layer, the introduction of a weight matrix can enable skipping of more than one layer,

leading to a variation known as HighwayNets [24, 25]. The structure of a Residual block is illustrated in Figure 8.

### 3. METHODOLOGY

#### 3.1 Proposed model

To identify the liver tumour in this study, deep learning algorithms will be used to a dataset. To segregate the liver and tumour, a fully convolutional neural network will be employed. Two ResUNets will be used: one to segment the liver and extract ROI, and the other to segment the tumour using the extracted ROI. The CT imaging dataset of patient given by IRCAD served as the training data for the learning models. Pre-processing has been used to divide the dataset into three smaller subsets: the training set, the validation set, and the testing set. The evaluation of the performance was done in terms of crucial metrics including Accuracy, Dice Coefficient, Confusion Matrix, and True Value Accuracy. Proposed workflow can be seen as in below Figure 9. Figure 10 represents CT slice before and after HU windowing.

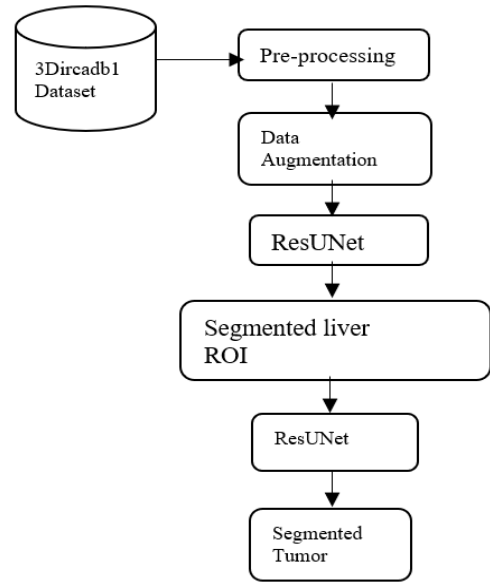


Figure 9. Overview of proposed workflow

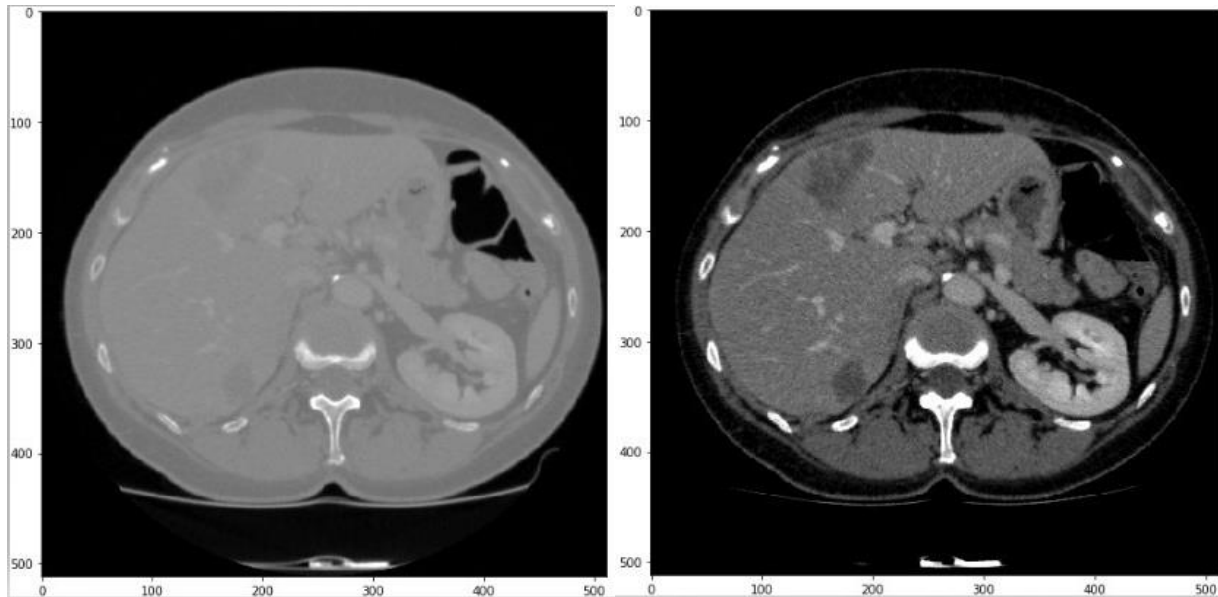


Figure 10. CT slice before and after HU windowing

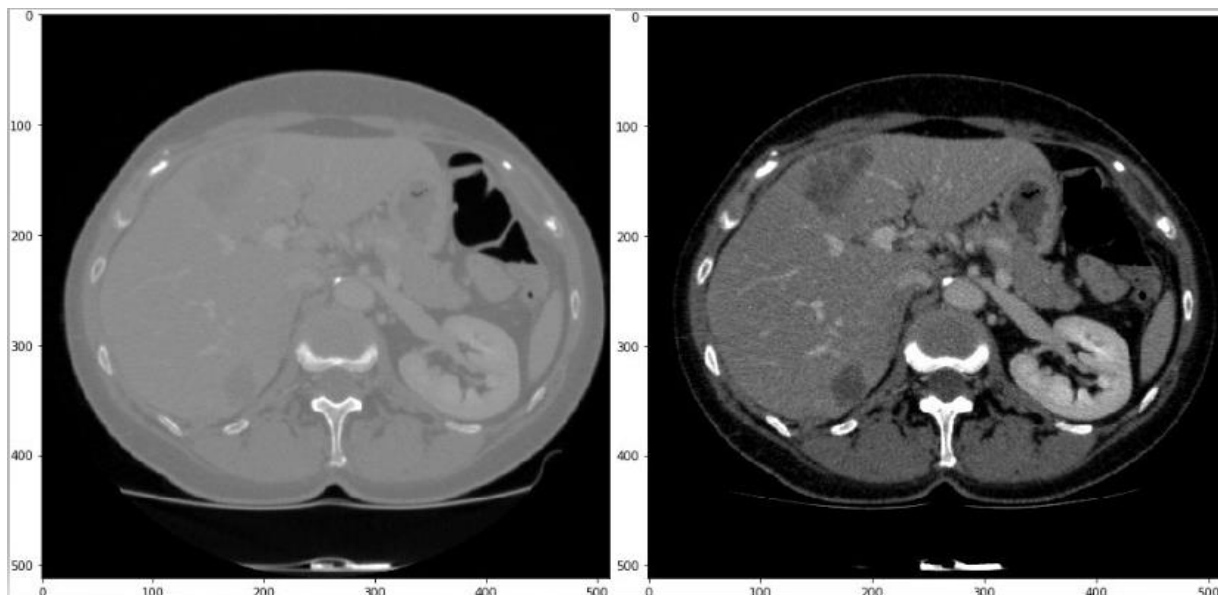


Figure 11. CT slice

### 3.2 Steps involved

#### Data Preprocessing

We Used 3D- IRCADb01 dataset and for every slice, in order to differentiate the liver from nearby Organs, we had to preprocess each slice.

#### Hounsfield Windowing

Hounsfield Unit (HU) is the average of the attenuation values of a certain voxel compared to the attenuation value of distilled water at standard temperature and pressure where the HU of water is zero and air is -1000. It is encoded in 12 bits thus have  $2^{12}$  values which is 4096 ranging from -1024 HU to 3071 HU table 3.1. It was named after the inventor of CT-scanning Sir Godfrey Newbold Hounsfield, and it's computed for any tissue as follows where  $\mu$  is the linear attenuation coefficient:

$$HU = \frac{1000 \times (\mu_{\text{tissue}} - \mu_{H_2O})}{\mu_{H_2O}}$$

#### Hisogram Equalization

Histogram Equalization (HE) is a method that is used to enhance the contrast in photographs, particularly when it is concentrated in a small area and is not evenly distributed.

Histogram To improve the contrast between the liver and figures of nearby organs, equalization was performed to the windowing image's output, then the image is normalized to ranges [0,1].

Figure 11 shows that before and after HU windowing & Histogram Equalization, the increase in contrast on the image on the right makes the tumors more visible and thus easier to segment.

#### Data Augmentation

We had to increase the dataset since our dataset had class imbalance issues because there were many more pixels without tumours than there were tumor-containing pixels. In order to increase training accuracy, prevent overfitting, and correct class imbalance, data augmentation is a technique that is often employed in various Deep Learning and Machine Learning applications. Data augmentation uses a variety of picture manipulation methods, including noise addition, rotation, cropping, and reflection. In this article, two methods were utilised to improve the data.

#### Merging Liver Tumors

Since the 3D-IRCADb01

Dataset contains tumor masks for every tumor on its own, we needed to merge all the different masks into 1 mask to facilitate the training and Augmentation of data Figures 12-14.



Figure 12. Mask for the first tumor

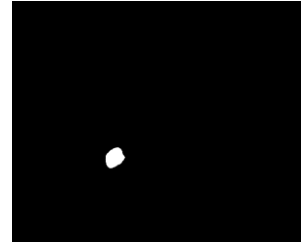


Figure 13. Mask for second tumor

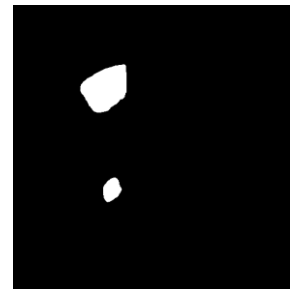


Figure 14. Final mask for both tumors merged together

#### Reflection

We reflect every slice that contains a tumor along the y-axis along with both the liver mask and tumor mask in order to increase the number of infected slices Figures 15-17.

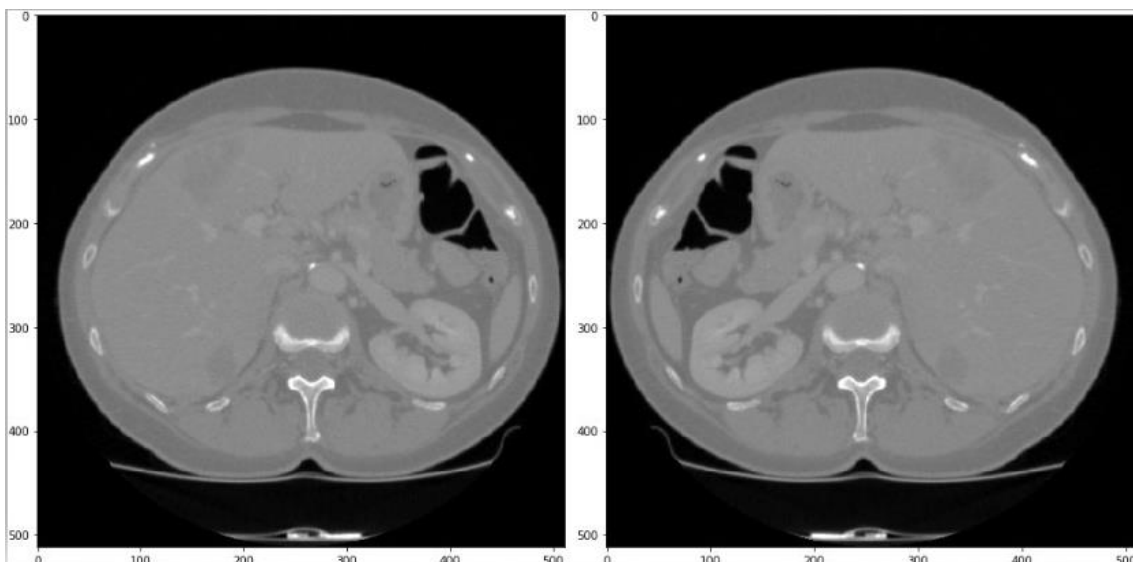


Figure 15. Slice before & after reflection

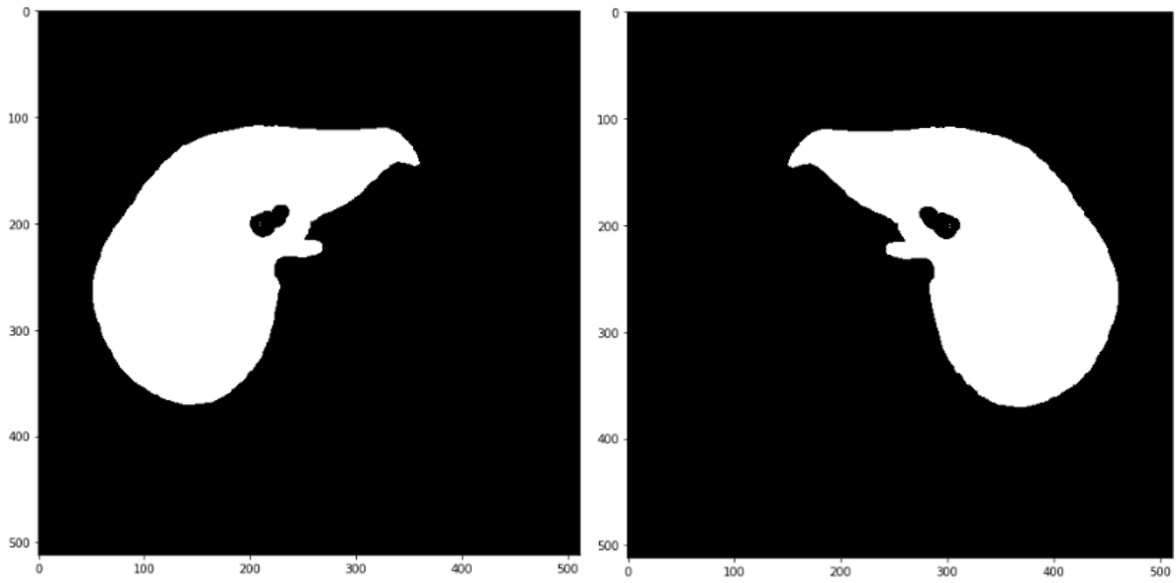


Figure 16. Liver mask before & after reflection

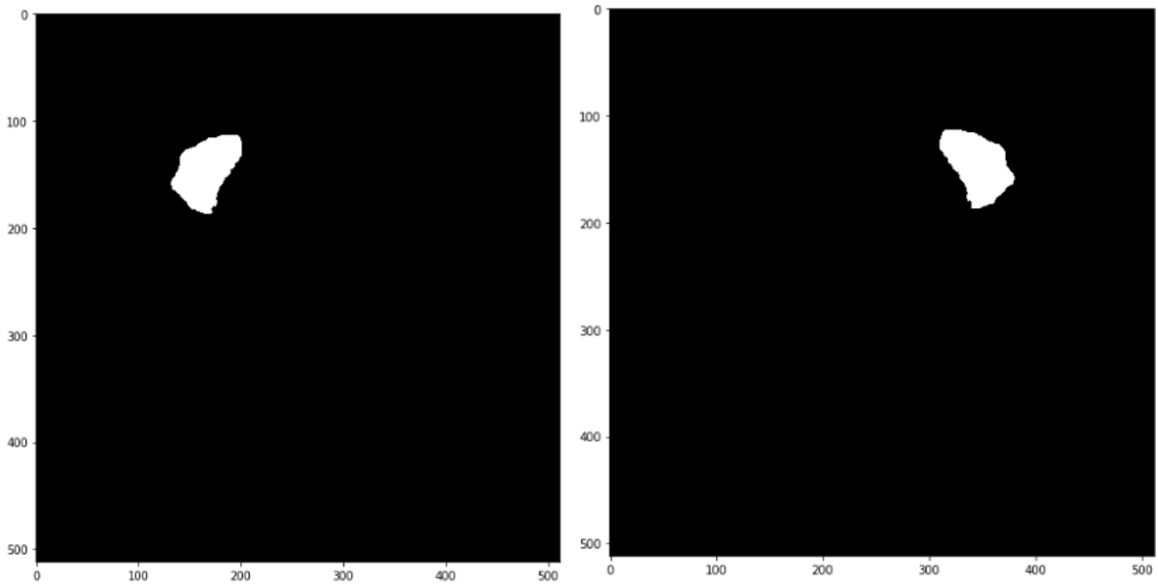


Figure 17. Tumor mask before & after reflection

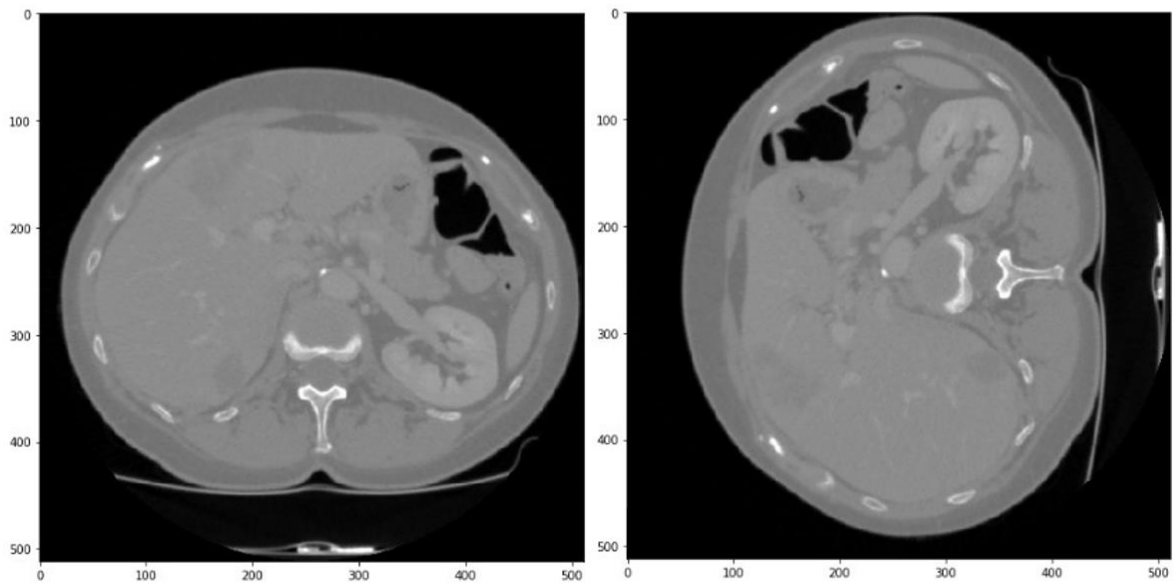
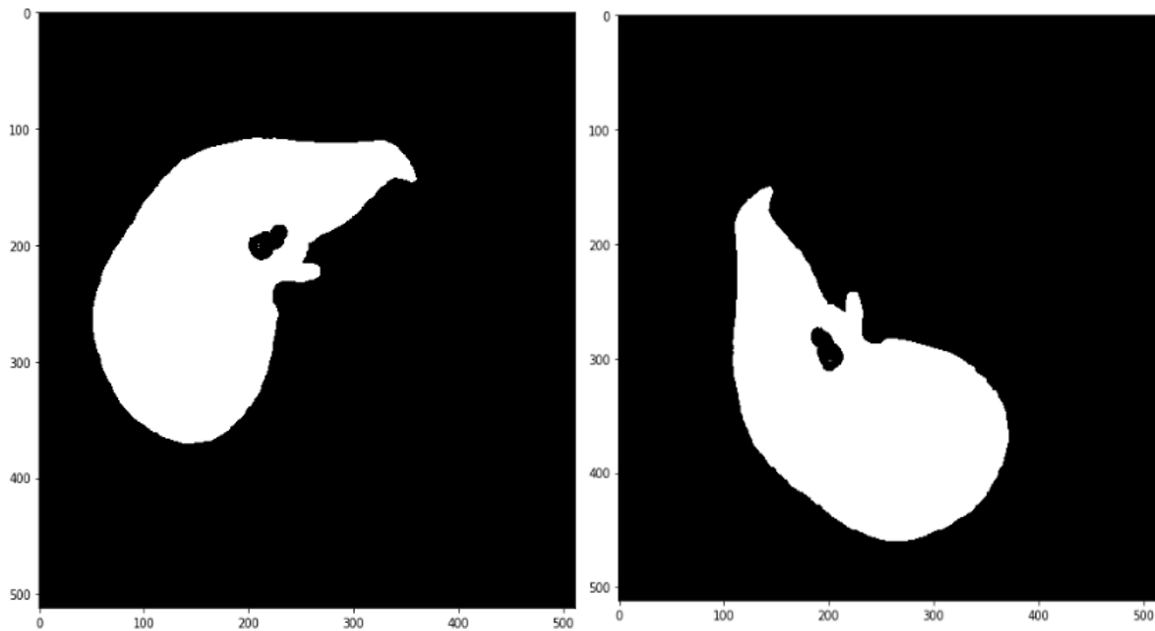
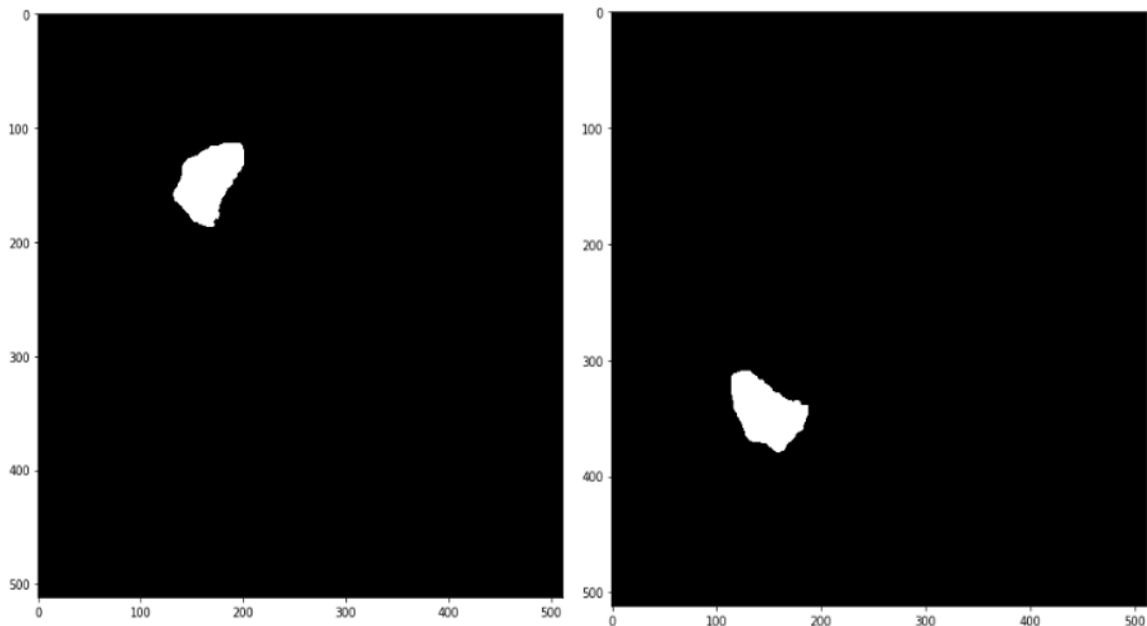


Figure 18. Slice before & after rotation 90°



**Figure 19.** Liver mask before & after rotation by 90°



**Figure 20.** Tumor mask before and after rotation

### Rotation

We rotate every slice that contains a tumor along with both the liver mask and tumor mask in order to increase the number of slices figures.

### ResUNet

By replacing convolutional blocks in the traditional U-Net and ResNet models with residual ones, ResUNet combines the advantages of both models. The residual unit, which requires fewer training parameters, will make it simpler to train the CNN, skip connections between the low and high levels of the network, and prevent degradation during information propagation inside the residual unit. Figures 18, 19, 20 represent slice, live mask, Tumor mask. Figure 21 represents ResUNet architecture.

The ResUNet is composed of three paths. There are three possible routes: encoding, which reduces the input to a

compact representation; decoding, which works in the opposite direction of encoding and categorizes the representation by pixel; and the bridge, which connects the two routes. Each route is built using Relative Units [26].

### Liver Segmentation

We use a CNN (ResUNet) for the sole purpose of Liver Segmentation. It is trained to recognise the Region of Interest using liver masks and CT scans (ROI) in order to segment the liver [27] and mask the neighboring like in Figures 22, 23.

### Tumor Segmentation

At first we used a U-Net to segment the tumors in the liver but got bad results so we tried using the ResUNet to segment the tumors. After removing the ROI from the initial CNN and the tumors' masks, it is trained on liver CT scans [26]. Examples in Figures 24-25.

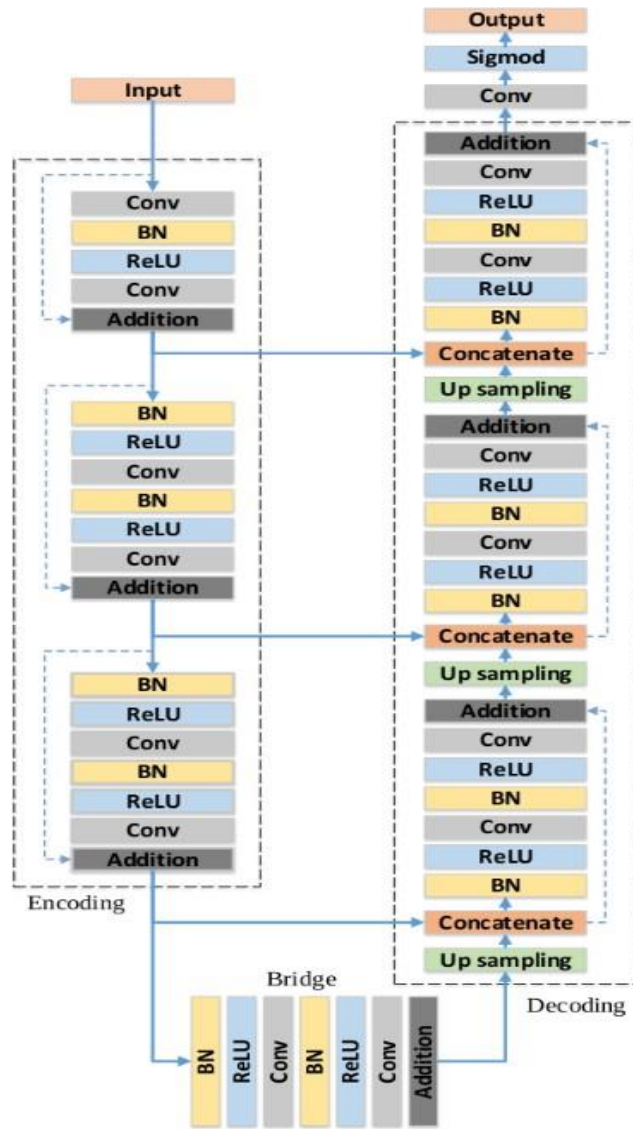


Figure 21. ResUNet architecture

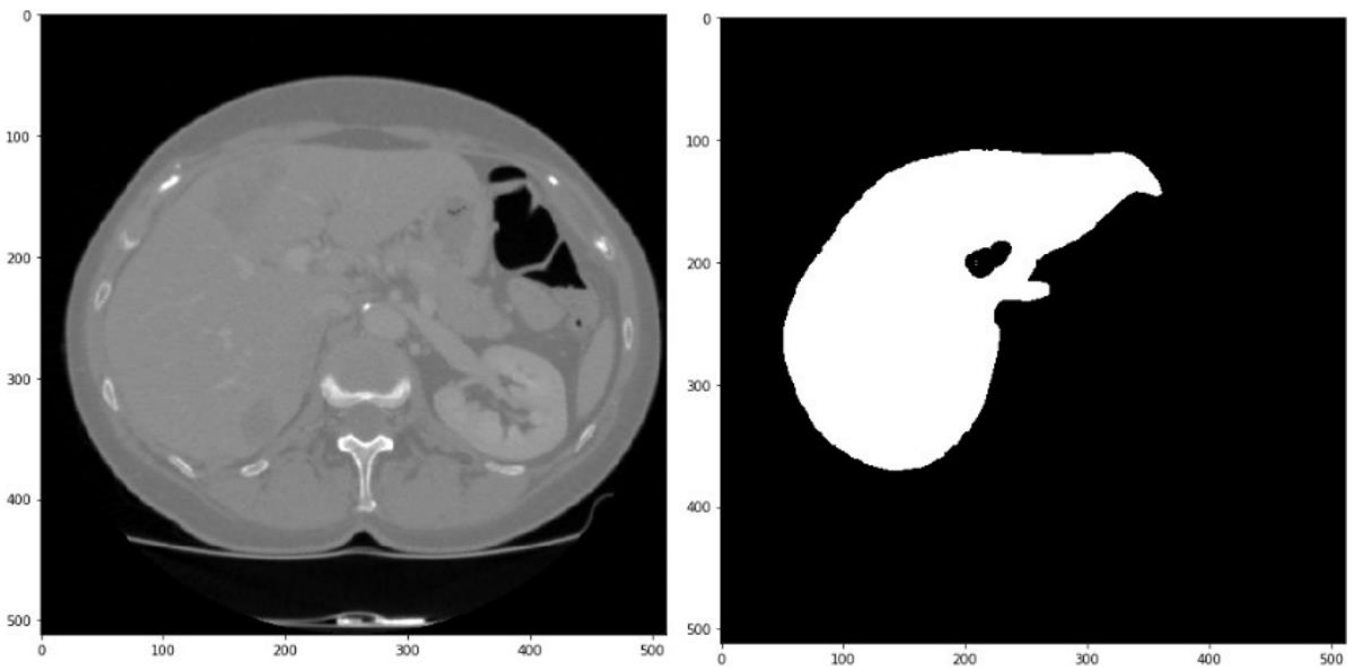


Figure 22. Liver Segmentation example

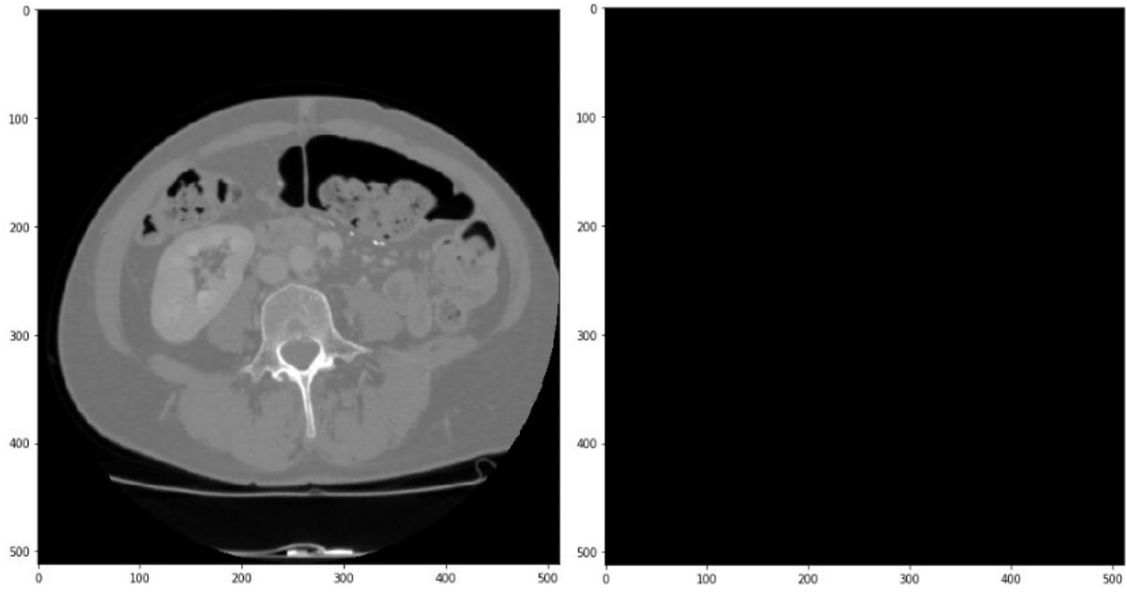


Figure 23. Liver segmentation without liver

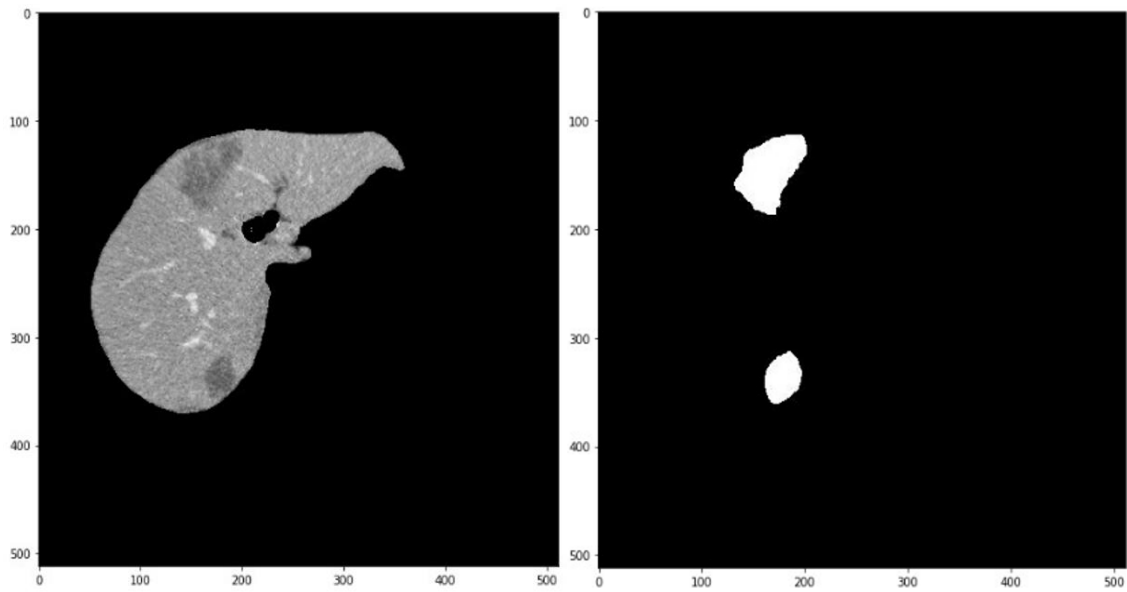


Figure 24. Tumor segmentation example

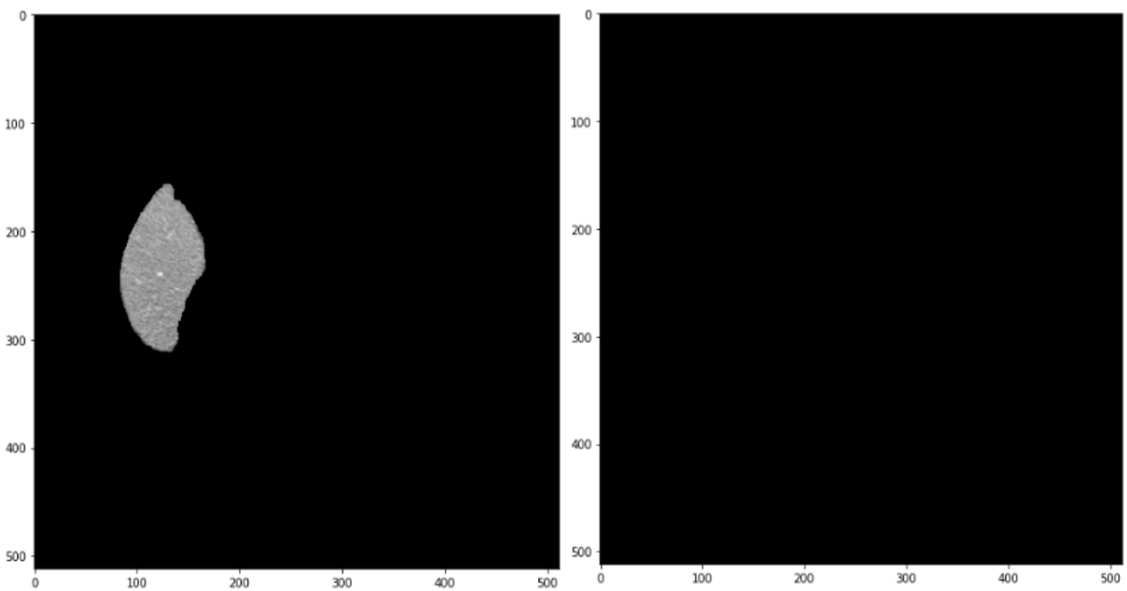


Figure 25. Liver has no tumor

## 4. RESULTS

### 4.1 Dataset

The datasets used in this research is 3D-IRCADb01 dataset made up of 3D CT scans of 10 men and 10 women, with liver tumours present in 75% of the cases, is made available to the public by the IRCAD Research Institute to fight stomach cancer. Each of the approximately 2,800 2D slices in the 3D CT scans, which are in the DICOM format, contains a mask for the liver, tumours, bones, arteries, kidneys, and lungs.

$$\text{Accuracy} = \frac{\text{True}^{\text{positive}} + \text{True}^{\text{negative}}}{\text{True}^{\text{positive}} + \text{True}^{\text{negative}} + \text{False}^{\text{positive}} + \text{False}^{\text{negative}}}$$

### Confusion Matrix

It calculates true positives, true negatives, false positives and false negatives then draws a heat-map of the results.

### 4.2 Evaluation parameters

In this research, we evaluate the performance of each of the learning models in terms of Accuracy, Dice coefficient, Confusion Matrix, True Value Accuracy.

#### Accuracy

Accuracy calculate how many pixels are classified correctly without any regard to the class, which is not a very good metric as the true negatives value will always be dominating by far and will always get 95%.

		Actual Class	
		1	0
Predicted Class	1	True Positive	False Positive
	0	False Negative	True Negative

#### Dice Coefficient

It calculates the overlap between the classes of the input A and predicted label B and is calculated as follows [28, 29].

$$\text{Dice} = \frac{2 \times |A \cap B|}{|A| + |B|}$$

#### True Value Accuracy

It calculates the accuracy of segmentation for tumors and the liver and is calculated as follows:

$$\text{True value Accuracy} = \frac{\text{TruePositives}}{\text{TruePositives} + \text{FalseNegatives}} \times 100$$

Computed tomography liver segmentation, formation, and segmentation of liver tumours Active contour classification models [28], Multiscale tumour candidates, and tumour candidates. For segmenting liver tumours, we suggested a number of machine learning techniques. Many CNNs have

been constructed for the segmentation of the liver and lesions application. For instance, the dataset for lesion identification is much less than the one for liver segmentation. Only manual 2D segmentation is possible for this data collection. Important to train essential invariants and effective network features when there are limited training samples available. We assess the effectiveness of our models using measures including accuracy, confusion matrix, Dice coefficient, and true value accuracy.

After using the ResUNet model to segment the Liver we got the following results.

**Table 1.** Dice coefficient results

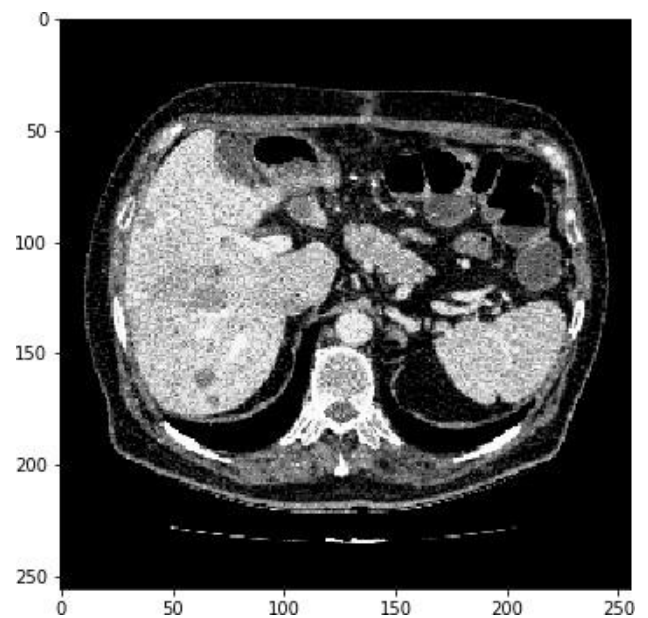
Epoch	Tumor Training Progress	
	Dice Coef	Valid Dice Coef
1	0.6377	0.2120
2	0.7155	0.7280
4	0.7572	0.7630
6	0.7749	0.5741
8	0.7886	0.8228
10	0.7897	0.7365
15	0.8131	0.8191
20	0.8268	0.8315
25	0.8437	0.8500
30	0.8523	0.8523
35	0.8607	0.7745
40	0.8683	0.7751
50	0.8838	0.8815

Table 1 explains Dice coefficient results for the ResUNet model for Liver Segmentation's training and validation data.

Here are the findings from our evaluation of a random sample of the validation data using the model.

Figures 26-27 show on the first random slice in figure. White pixels have livers, but black pixels don't, as seen by the true label on the left and the anticipated label on the right.

An accuracy of 99.4% and a true value accuracy of 98.1% were attained by one of the random samples (fig). Figure 27 shows the anticipated liver and Figure 28 shows the Confusion Matrix.



**Figure 26.** CT slice of the first random sample before liver segmentation

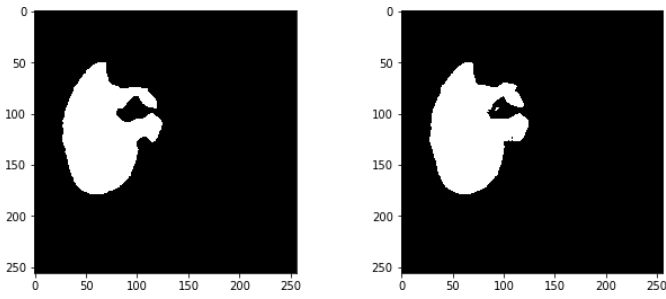


Figure 27. Result of liver segmentation

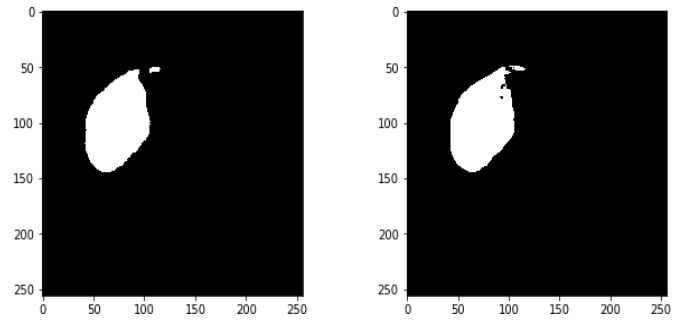


Figure 30. Result of liver segmentation

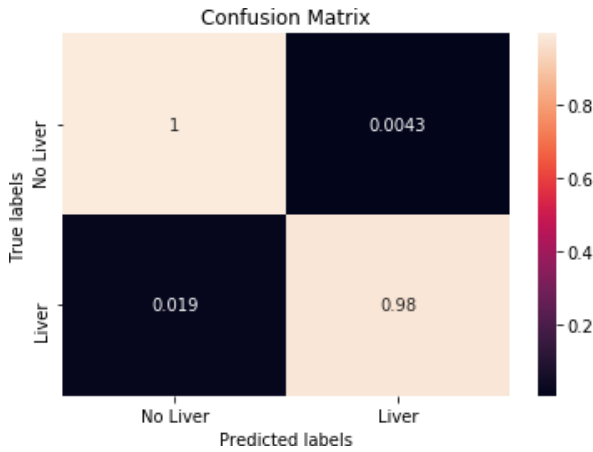


Figure 28. Confusion matrix

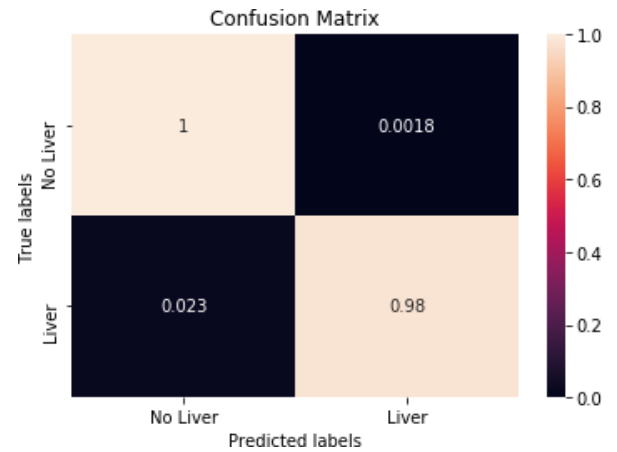


Figure 31. Confusion matrix

Figure 28 says Confusion Matrix following liver segmentation from the expected value of the first slice in the figure:

- A different random sample (fig) had an accuracy of 99.6% and a true value accuracy of 97.6%.
- We can see the predicted liver in Figure 29 and the Confusion Matrix in Figure 28.

The ResUNet showed some limitations as it failed to diagnose very small tumors.

One of the failing samples achieved an Accuracy of 99.95% and a True Value Accuracy of 0%. We can see the failure in Figure 30 and the Confusion Matrix in Figure 31.

Result of tumor segmentation on slice in Figure 32.

True label White pixels represent tumours on the left and right, while black pixels represent tumor-free pixels.

It is obvious that the tumor was not predicted by the model at all and also some tumors have less true value accuracy.

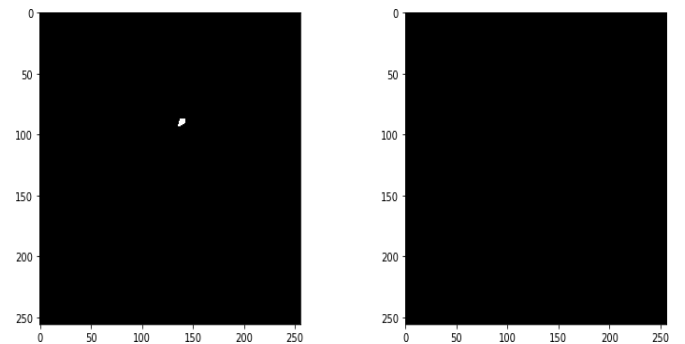


Figure 32. Result of tumor segmentation

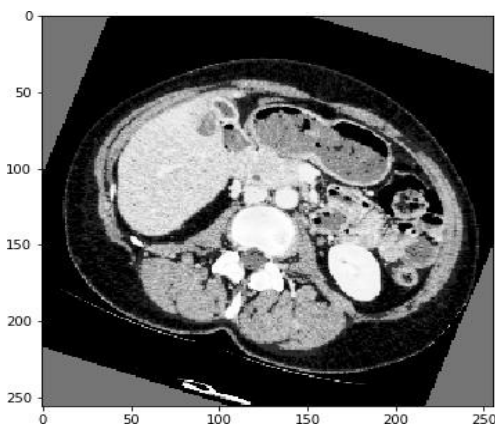


Figure 29. Random example of a CT slice before to liver segmentation

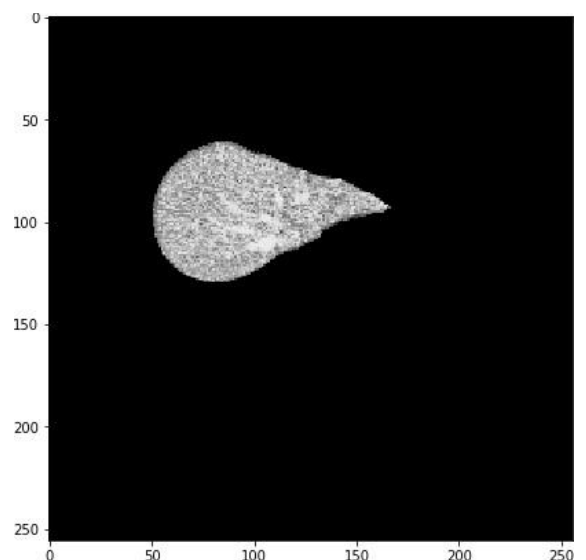
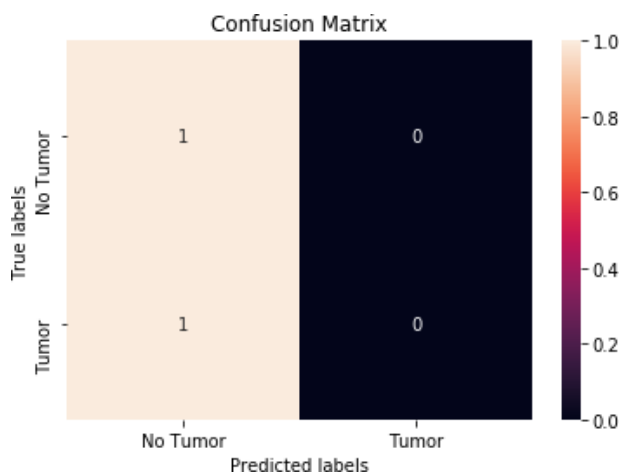


Figure 33. A sample CT slice with the liver mask



**Figure 34.** Confusion matrix

Figures 33 and 34 represents sample CT slice with the liver mask and Confusion matrix respectively.

## 5. CONCLUSIONS AND FUTURE SCOPE

In this work, the liver and liver tumours were automatically segmented pixel-by-pixel from CT images using the ResUNet model. We were successful in attaining our goals, as shown by the data, and CNNs are among the best techniques for segmenting liver cancers. They should be studied on cancer types other liver tumours, and ResUNet shown excellent promise.

There are several restrictions notwithstanding the ResUNet's highly encouraging outcomes. We might be able to overcome these limitations by training for further epochs, using more data, alternate datasets, or different preprocessing techniques.

## REFERENCES

[1] Abdel-Misih, S.R., Bloomston, M. (2010). Liver anatomy. *Surgical Clinics*, 90(4): 643-653. <https://doi.org/10.1016/j.suc.2010.04.017>

[2] Bray, F., Ferlay, J., Soerjomataram, I., Siegel, R.L., Torre, L.A., Jemal, A. (2018). Global cancer statistics 2018: GLOBOCAN estimates of incidence and mortality worldwide for 36 cancers in 185 countries. *CA: A Cancer Journal for Clinicians*, 68(6): 394-424. <https://doi.org/10.3322/caac.21492>

[3] Mustafa, N., Abdul Razak, N.H.S., Abu Talip Yusof, N., Abdul Karim, M.S. (2021). Development of microwave antenna for cancer treatment. In *Advances in Robotics, Automation and Data Analytics: Selected Papers from iCITES 2020*, pp. 127-136. [https://doi.org/10.1007/978-3-030-70917-4\\_14](https://doi.org/10.1007/978-3-030-70917-4_14)

[4] Power, S.P., Moloney, F., Twomey, M., James, K., O'Connor, O.J., Maher, M.M. (2016). Computed tomography and patient risk: Facts, perceptions and uncertainties. *World Journal of Radiology*, 8(12): 902.

[5] Carleton, P.F., Schachter, S., Parrish, J.A., Collins, J.M., Crocker, J.B., Dixon, R.F., Lash, T.B. (2016). National institute of biomedical imaging and bioengineering point-of-care technology research network: Advancing precision medicine. *IEEE Journal of Translational*

*Engineering in Health and Medicine*, 4: 1-14. <https://doi.org/10.1109/JTEHM.2016.2598837>

[6] Bai, Z., Jiang, H., Li, S., Yao, Y.D. (2019). Liver tumor segmentation based on multi-scale candidate generation and fractal residual network. *Ieee Access*, 7: 82122-82133. <https://doi.org/10.1109/ACCESS.2019.2923218>

[7] Das, A., Acharya, U.R., Panda, S.S., Sabut, S. (2019). Deep learning based liver cancer detection using watershed transform and Gaussian mixture model techniques. *Cognitive Systems Research*, 54: 165-175. <https://doi.org/10.1016/j.cogsys.2018.12.009>

[8] Chlebus, G., Schenk, A., Moltz, J.H., van Ginneken, B., Hahn, H.K., Meine, H. (2018). Deep learning based automatic liver tumor segmentation in CT with shape-based post-processing. <https://openreview.net/pdf?id=rJccgk3iM>.

[9] Li, W., Jia, F., Hu, Q. (2015). Automatic segmentation of liver tumor in CT images with deep convolutional neural networks. *Journal of Computer and Communications*, 3(11): 146-151. <http://dx.doi.org/10.4236/jcc.2015.311023>

[10] Ben-Cohen, A., Diamant, I., Klang, E., Amitai, M., Greenspan, H. (2016). Fully convolutional network for liver segmentation and lesions detection. In *Deep learning and data labeling for medical applications*, pp. 77-85. [http://dx.doi.org/10.1007/978-3-319-46976-8\\_9](http://dx.doi.org/10.1007/978-3-319-46976-8_9)

[11] Christ, P.F., Ettliger, F., Grün, F., et al. (2017). Automatic liver and tumor segmentation of CT and MRI volumes using cascaded fully convolutional neural networks. *arXiv preprint arXiv:1702.05970*. <https://doi.org/10.48550/arXiv.1702.05970>

[12] Goryawala, M., Guillen, M.R., Cabrerizo, M., Barreto, A., Gulec, S., Barot, T.C., Adjouadi, M. (2011). A 3-D liver segmentation method with parallel computing for selective internal radiation therapy. *IEEE Transactions on Information Technology in Biomedicine*, 16(1): 62-69. <https://doi.org/10.1109/TITB.2011.2171191>

[13] Milletari, F., Navab, N., Ahmadi, S.A. (2016). V-net: Fully convolutional neural networks for volumetric medical image segmentation. In *2016 fourth international conference on 3D vision (3DV)*, pp. 565-571. <https://doi.org/10.1109/3DV.2016.79>

[14] Yuan, Y. (2017). Hierarchical convolutional-deconvolutional neural networks for automatic liver and tumor segmentation. *arXiv preprint arXiv: 1710.04540*. <https://arxiv.org/abs/1710.04540>

[15] Chlebus, G., Meine, H., Moltz, J.H., Schenk, A. (2017). Neural network-based automatic liver tumor segmentation with random forest-based candidate filtering. *arXiv preprint arXiv: 1706.00842*. <https://arxiv.org/abs/1706.00842>

[16] Han, X. (2017). Automatic liver lesion segmentation using a deep convolutional neural network method. *arXiv preprint arXiv: 1704.07239*. <https://arxiv.org/abs/1704.07239>

[17] Ben-Cohen, A., Klang, E., Kerpel, A., Konen, E., Amitai, M.M., Greenspan, H. (2018). Fully convolutional network and sparsity-based dictionary learning for liver lesion detection in CT examinations. *Neurocomputing*, 275: 1585-1594. <https://doi.org/10.1016/j.neucom.2017.10.001>

[18] Ronneberger, O., Fischer, P., Brox, T. (2015). U-net: Convolutional networks for biomedical image segmentation. In *International Conference on Medical*

- Image Computing and Computer-Assisted Intervention, pp. 234-241. [https://doi.org/10.1007/978-3-319-24574-4\\_28](https://doi.org/10.1007/978-3-319-24574-4_28)
- [19] Hassanzadeh, T., Essam, D., Sarker, R. (2020). Evou-net: an evolutionary deep fully convolutional neural network for medical image segmentation. In Proceedings of the 35th Annual ACM Symposium on Applied Computing, pp. 181-189. <https://doi.org/10.1145/3341105.3373856>
- [20] Zhang, Z., Liu, Q., Wang, Y. (2018). Road extraction by deep residual u-net. *IEEE Geoscience and Remote Sensing Letters*, 15(5): 749-753. <https://doi.org/10.1109/LGRS.2018.2802944>
- [21] Zou, K.H., Warfield, S.K., Bharatha, A., Tempany, C.M., Kaus, M.R., Haker, S.J., Kikinis, R. (2004). Statistical validation of image segmentation quality based on a spatial overlap index1: Scientific reports. *Academic Radiology*, 11(2): 178-189. [https://doi.org/10.1016/S1076-6332\(03\)00671-8](https://doi.org/10.1016/S1076-6332(03)00671-8)
- [22] Pizer, S.M., Amburn, E.P., Austin, J.D., Cromartie, R., Geselowitz, A., Greer, T., Zuiderveld, K. (1987). Adaptive histogram equalization and its variations. *Computer Vision, Graphics, and Image Processing*, 39(3): 355-368. [https://doi.org/10.1016/S0734-189X\(87\)80186-X](https://doi.org/10.1016/S0734-189X(87)80186-X)
- [23] Hong, J.S., Kaneko, T., Sekiguchi, R., Park, K.H. (2001). Automatic liver tumor detection from CT. *IEICE Transactions on Information and Systems*, 84(6): 741-748.
- [24] What is Rectified Linear Unit (ReLU)? Introduction to ReLU Activation Function. <https://www.mygreatlearning.com/blog/relu-activation-function/>, accessed on 25 August 2023.
- [25] ul Haq, M.S., Irtaza, A., Nida, N., Shah, M.A., Zubair, L. (2021). Liver tumor segmentation using resnet based Mask-R-CNN. *International Bhurban Conference on Applied Sciences and Technology*. <https://doi.org/10.1109/IBCAST51254.2021.9393194>
- [26] 3D-Liver-Segmentation. <https://github.com/fshnkarimi/3D-Liver-Segmentation>, accessed on 25 August 2023.
- [27] Sang, S., Xing, L. (2023). Automated small tumor segmentation by a template-based global hierarchical attention method. *International Journal of Radiation Oncology, Biology, Physics*, 117(2): e485. <https://doi.org/10.1016/j.ijrobp.2023.06.1712>
- [28] Evaluating Deep Learning Models: The Confusion Matrix, Accuracy, Precision, and Recall. <https://www.kdnuggets.com/2021/02/evaluating-deep-learning-models-confusion-matrix-accuracy-precision-recall.html>, accessed on 25 August 2023.
- [29] How to Configure Image Data Augmentation in Keras. <https://machinelearningmastery.com/how-to-configure-image-data-augmentation-when-training-deep-learning-neural-networks/>, accessed on 25 August 2023.